MINISYMPOSIUM

PET imaging in pediatric neuroradiology: current and future applications

Sunhee Kim · Noriko Salamon · Hollie A. Jackson · Stefan Blüml · Ashok Panigrahy

Abstract Molecular imaging with positron emitting tomography (PET) is widely accepted as an essential part of the diagnosis and evaluation of neoplastic and non-neoplastic disease processes. PET has expanded its role from the research domain into clinical application for oncology, cardiology and neuropsychiatry. More recently, PET is being used as a clinical molecular imaging tool in pediatric neuroimaging. PET is considered an accurate and noninvasive method to study brain activity and to understand pediatric neurological disease processes. In this review, specific examples of the clinical use of PET are given with respect to pediatric neuroimaging. The current use of co-registration of PET with MR imaging is exemplified in regard to pediatric epilepsy. The current use of PET/CT in the evaluation of head and neck lymphoma and pediatric brain tumors is also reviewed. Emerging technologies including PET/MRI and neuroreceptor imaging are discussed.

Keywords PET/CT · Pediatric brain tumors · Lymphoma · Epilepsy

S. Kim · A. Panigrahy (✉)
Department of Radiology,
Children's Hospital of Pittsburgh of UPMC,
Children's Hospital Drive, 45th Street and Penn Avenue,
Pittsburgh, PA 15201, USA
e-mail: panigrahya@upmc.edu

N. Salamon
Department of Radiology, Ronald Reagan UCLA Medical Center,
UCLA David Geffen School of Medicine at UCLA,
Los Angeles, CA, USA

H. A. Jackson · S. Blüml · A. Panigrahy
Department of Radiology, Childrens Hospital Los Angeles,
Keck School of Medicine of USC,
Los Angeles, CA, USA

Introduction

Positron emission tomography (PET) imaging is based on the detection of photons that arise from the decay of injected radiotracers. With the ability to image various radiotracers in the brain, it is possible to follow molecular interactions and pathways. PET scanning can provide assessment of physiological and pathophysiological processes and can measure chemical changes that occur before they are visible on CT and MRI. PET does have some disadvantages including radiation exposure (comparable to CT), limited availability and possible need for sedation in some children. In this review, selected topics that are relevant to the use of PET imaging in pediatric neuroimaging are discussed including quantitation of PET, brain development and PET, PET imaging in epilepsy (including image co-registration with MR) and PET imaging in pediatric neuro-oncology (including PET/CT of head and neck lymphoma and pediatric brain tumors). Emerging applications of PET including combined PET/MR imaging and neuroreceptor imaging are discussed at the end of the review.

Quantification in PET imaging

One of the major advantages of PET is its ability to quantify radioactivity concentration within a given region of interest. To provide meaningful information on available receptor binding sites or biochemical processes, the tracer activity and its distribution need to be analyzed quantitatively. There are three categories of methods in analyzing data: (1) qualitative analysis (visual assessment), (2) semiquantitative assessment such as standardized uptake value (SUV) and lesion-to-background (L:B) ratio and (3) absolute quantitative analysis using nonlinear regression, Patlak graphical analysis and

simplified quantitative methods [1]. Qualitative analysis requires minimal effort with least accuracy, whereas an absolute quantification method requires compartmental kinetic modeling to measure the individual rate constant based on data from dynamic image acquisition and serial blood sampling. This method is complex and time-consuming and therefore is impractical in most clinical settings.

SUV is the most commonly used semi-quantitative parameter in clinical fluorodeoxyglucose (FDG) PET studies. SUV is defined by lesion concentration of tracer per injected dose of normalized patient body weight multiplied by a decay factor.

$$SUV = \frac{\text{Tissue activity concentration (MBq/ml)}}{(\text{Injected dose(MBq/ml)}/\text{Body weight(g)} \times \text{Decay factor of }^{18}\text{F})}$$

Compared to complicated and time-consuming kinetic modeling, the SUV calculation is simple without any need for arterial blood sampling and faster without dynamic image acquisition. It is also known that tissue SUV has a linear relationship with the rate of glucose metabolism measured by kinetic modeling with high correlation coefficients of 0.91 and 0.84, respectively [2, 3]. Many factors affect the outcome of SUV. These factors can be broadly categorized as technical, biological and physical. Technical errors include relative calibration between PET scanner and dose calibrator [4, 5], residual activity in syringe or administration system, incorrect decay correction resulting from inaccurate synchronization of PET camera and dose calibrator, and incorrect time interval between injection and calibration time [6]. Biological errors include blood glucose level [7–9], uptake period [10], inflammation process near tumor [11], and patient motion or breathing [12]. Physical errors include scan-acquisition parameter affecting signal-to-noise ratio [5], image-reconstruction parameter such as resolution and partial-volume effect [5], size and type of region of interest (ROI) [5, 6], normalization factor for SUV such as body weight, body surface area, mean body weight [7], blood glucose level correction [7–9] and overestimation of attenuation and SUV in the presence of a contrast agent.

Although many factors have a relatively small effect (<15%) on SUV outcome, on average the sum of many factors can make significant difference in SUV outcome [6]. Therefore, standardization of protocol is critical for an accurate and reproducible SUV measurement and quantification.

PET and brain development

Functional development of the pediatric brain has been evaluated by FDG-PET. Chugani et al. [13] demonstrated that the metabolic pattern of a developing brain follows the order of anatomical, evolutional and behavioral development. Increased glucose metabolism is shown in the visual, sensorimotor cortex and the cerebellum, and this is correlated with early visuo-spatial and sensorimotor function and primitive reflexes. Hypermetabolism in the basal ganglia is known to be associated with developing movement and sensorimotor function.

The quantitative analysis of brain FDG-PET has demonstrated that the degree of glucose metabolism of infants is significantly lower than that of adults. The degree of metabolic activity of neonates is about 30% that of adults and it continues to increase with age. It is hypothesized that increased metabolism is associated with increased metabolic demands from neuronal plasticity development [14]. By a child's third year, the metabolic level exceeds that of adults, and it reaches its plateau between ages 4 and 9 with a value 1.3 times higher than that of normal adults [15]. After this period, the value decreases to adult level by the end of the second decade [13]. Loessner et al. [16] showed significant decline in overall degree of cortical metabolism, which was a consistent finding related with normal aging in a study of 120 healthy volunteers between the ages of 17 and 79.

The pattern of glucose metabolism of a pediatric brain becomes similar to that of young adults by 1 year of age. Compared to other parts of the brain, the frontal lobe demonstrates more significant age-related metabolic changes. For the first 4 months of life, the glucose metabolism in the frontal lobe remains relatively low and gradually increases as frontal lobe-mediated cognitive function and complicated social interaction develops. Linear regression analysis by Chawluk et al. [17] demonstrated 38% decrease in the whole brain metabolism with aging and 42% decline in frontal lobe metabolism. No significant differences were found between men and women in regional glucose metabolism [16, 18]. Other cortical areas such as the parietal, occipital, and temporal lobes have significant variations within and across age groups. It is shown that metabolic activity in the basal ganglia, thalami, hippocampi, cerebellum, visual cortices, and posterior cingulated gyrus remain stable throughout age [16]. The metabolic activity in the brainstem increases with age [16]. It is not clear whether brain atrophy contributes to this hypometabolism with aging. Further brain FDG-PET studies need to be done with consideration of atrophy correction.

PET in pediatric epilepsy

A number of PET tracers make it possible to visualize different aspects of brain function such as blood flow, glucose metabolism, protein synthesis, and neurotransmission. F-18

FDG is the most widely used PET tracer for evaluating brain glucose metabolism for localizing epileptogenic focus in clinical practice. Because of its long uptake period (40–60 min), FDG-PET is more suitable for capturing the interictal state of epilepsy rather than the ictal state. The pattern of glucose metabolism in a PET scan is hypometabolism of the ipsilateral temporal lobe with or without less severe hypometabolism in the extratemporal structures such as frontal lobe, parietal lobe and contralateral temporal lobe. If lesions are associated with epilepsy, the extent of hypometabolism is greater than the size of the structural lesion [19].

The pathophysiology of regional hypometabolism in interictal FDG-PET is not clear. Several hypotheses have been proposed, including neuronal cell loss, neuronal inhibition, and diaschisis associated with hippocampal neuronal loss [20]. However, conflicting evidence also exists, such as temporal hypometabolism without neuronal loss or gliosis [21], and the poor correlation between metabolic change in the temporal lobe and hippocampal cell count [22]. Additional factors that might contribute to interictal hypometabolism include an inhibitory process and reduction in synaptic density. It has been suggested that this secondary inhibition or neuronal loss in the area surrounding the epileptic zone can cause larger and more extensive hypometabolism in FDG-PET [20, 23, 24] and hypoperfusion in single photon emission CT (SPECT) [25] than the area of involvement seen on electroencephalography (EEG) or pathologic correlate. Further work needs to be done to validate this pathophysiology.

It has been demonstrated that interictal FDG-PET is more sensitive than MRI in localizing epileptogenic focus in both temporal and extra-temporal epilepsy [26]. It was reported that about 29% of patients with partial epilepsy have a normal MRI [27]. Intracranial EEG is limited in this situation by the lack of knowledge needed to target electrode locations to the areas of suspected seizure onset. The potential diagnostic role of FDG-PET and SPECT in the absence of anatomical findings has been described by Lee et al. [28], and they showed more than 70% of positive predictive value of FDG-PET and ictal SPECT in MRI-negative cryptogenic epilepsy. Chugani et al. [29] and Swartz et al. [30] also showed localization rates of 57% and 32%, respectively, by FDG-PET in patients with normal MRI.

MRI and PET co-registration in pediatric epilepsy

18F-FDG-PET represents a useful tool for presurgical evaluation of epilepsy, particularly when MRI is nonlesional. Previous studies have shown 18F-FDG-PET to have 63–100% sensitivity in lateralizing temporal lobe epilepsy

(TLE) and to provide complementary information to MRI [31–33]. For extratemporal lobe epilepsy (ETLE), studies have shown 18F-FDG-PET to have slightly lower sensitivity at 36–83% [33, 34]. In addition to increasing detection rates, some studies have indicated that 18F-FDG-PET can provide postsurgical prognostic information independent of information provided by MRI [35]. 18F-FDG-PET might thus provide complementary as well as supplementary functional information in regard to the etiology of seizure activity [29, 36] (Figs. 1 and 2).

Given the parallel roles of MRI and 18F-FDG-PET in presurgical evaluation for epilepsy patients, co-registration of MRI and 18F-FDG-PET might enhance presurgical management of intractable epilepsy. This has not been unequivocally established, but it is already recommended that 18F-FDG-PET images be interpreted in light of all structural imaging information [37]. In the recent UCLA cohort, 18F-FDG-PET and MRI co-registration demonstrated favorable postsurgical outcomes (Engel class I–II) in 80% of the patients with intractable epilepsy with the application of co-registered imaging to maximally resect the functionally abnormal area. This technique uses anatomic imaging to help define the limits of resection, despite previous MRI findings that had been considered to be nonlesional [38]. In comparison, in studies of patients without the use of anatomic and functional co-registration, only 69–76% of patients were Engel class I–II at a similar follow-up period, 30–50% when preoperative MRI was nonlesional [39]. Reasons for this lower rate of favorable outcomes without co-registered image-guided surgery include difficulty in delineating the epileptogenic zone and correlating it with relevant structural anatomy [39].

Application to focal cortical dysplasia (FCD)

In the most widely accepted histopathologic classification system, FCD is divided into two subtypes: type I and type II [40, 41]. FCD type II is associated histopathologically with dysmorphic or dysplastic neurons, often with balloon cells. MRI of FCD type II shows focal cortical thickening, abnormal gyral and sulcal patterns, and prominent blurring of the gray-white matter junction. FCD type I is associated with architectural abnormalities, often with giant or immature neurons. MRI of FCD type I shows less prominent gray-white matter junction blurring, and signal changes predominantly in white matter and prominent lobar hypoplasia [42]. MRI of FCD type I has been challenging, despite improvements in recent MRI techniques, as it usually yields only normal or subtly abnormal MRI findings. Studies have demonstrated that only 30–70% of patients with type I FCD have positive MRI scans, compared with 80–100% of those with type II FCD [43, 44].
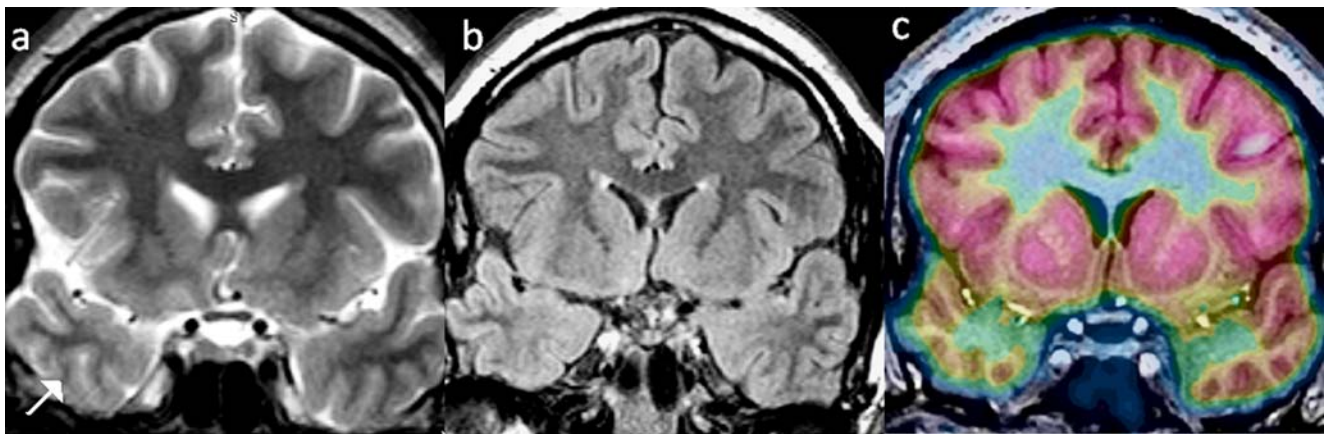
Fig. 1 In a child being evaluated for epilepsy, the coronal T2 image (a) and coronal FLAIR (b) show mild volume loss in the right anterior temporal lobe. c The PET-fusion MR image shows hypometabolism with the right anterior temporal lobe. The pathology after surgical resection of the right anterior temporal lobe was focal cortical dysplasia type 1

In comparison, 18F-FDG-PET has been shown to effectively identify FCD despite normal MRI findings [29]. 18F-FDG-PET has been reported to be 75–100% sensitive in localizing areas with FCD, when taken as a group [45]. But for subtle FCD, MRI identified only 13% as compared to 86% with 18F-FDG-PET. This study suggests that 18F-FDG-PET is more sensitive than MRI and that it is particularly useful in cases of type I FCD.

Application to tuberous sclerosis complex (TSC)

TSC is an autosomal-dominant neurocutaneous syndrome with manifestations found throughout the body. In the brain, disordered proliferation, migration, and differentiation of neurons results in subependymal giant-cell astrocytomas, subependymal nodules and tubers. Starting at infancy, children with TSC develop increasing seizures, and 25–50% of TSC patients develop intractable epilepsy [46]. Usually, multiple tubers are present, but seizures often arise from a single tuber [47]. Given the medically refractory nature of the epilepsy, surgery should be considered for such cases. The outcome of surgery is dependent on accurate preoperative assessment to guide resection of the epileptogenic tuber [48].

But presurgical evaluation has been challenging. Although CT and MRI can reveal the presence of multiple tubers, such anatomic imaging used alone cannot select the epileptogenic tuber. Additionally, there are cases of TSC patients with intractable epilepsy in which MRI fails to detect histopathologically demonstrated tubers [49]. Furthermore,
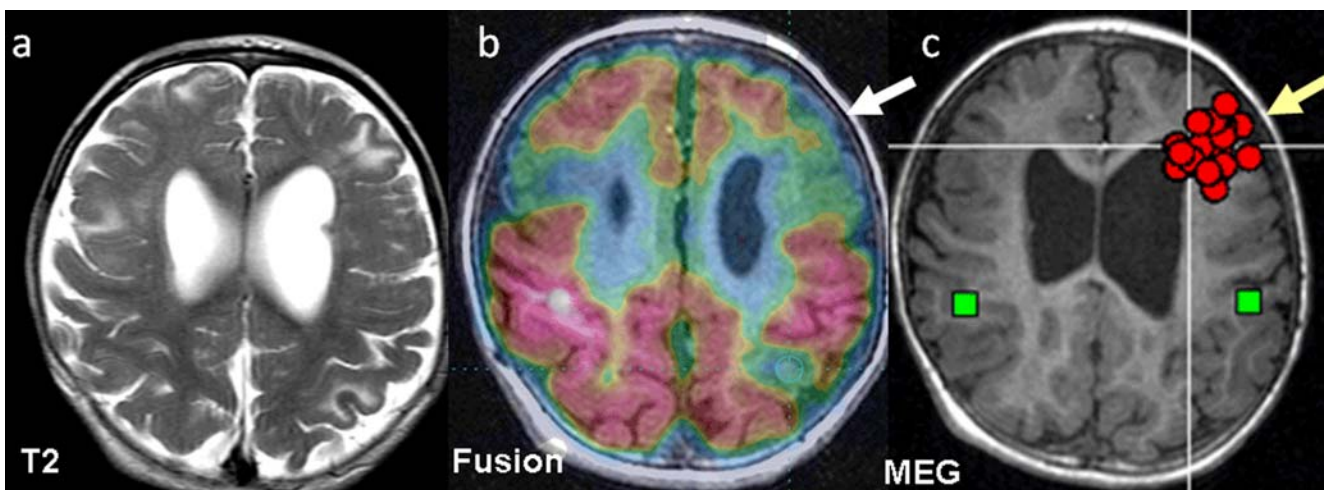

Fig. 2 In a child with tuberous sclerosis, the axial T2 image (a) shows multiple subcortical lesions that correspond to tubers. b The PET-MR fusion image shows multiple areas of hypometabolism in the frontal lobes bilaterally and also the left parietal lobe. c The MEG study shows abnormal activity in the left frontal lobe tuber

noninvasive EEG techniques might not localize epileptogenic activity to a discrete tuber. Recently, a multimodality imaging approach using MRI and 18F-FDG-PET co-registration as well as DTI has been demonstrated to be useful in presurgical evaluation to localize epileptogenic tubers [50]. Larger volumes of 18F-FDG-PET interictal hypometabolism relative to MRI tuber size showed promise for detecting epileptogenic tubers as well as improving surgical outcomes [50]. Thus a multimodality approach with MRI and 18F-FDG-PET co-registration should continue to be evaluated as a promising technique for noninvasive presurgical evaluation for TSC.

PET/CT in pediatric head and neck lymphoma

CT plays an important role in the initial staging and evaluation of recurrence of various pediatric oncologic diseases. While CT may provide excellent anatomic and morphologic information related to the extent of metastatic disease, it is limited in differentiating benign from malignant lesions in lymphoma or primary organs. Whole-body PET with 18F-FDG can provide excellent detection of malignant lesions and has been shown to be effective in the management of many different adult oncologic diseases. 18F-FDG can also be taken up by normal physiological processes and inflammatory processes that are non-neoplastic. Recently, combined PET/CT imaging has been introduced and recent studies have proven that it may improve the diagnostic accuracy of staging adult oncologic diseases [51–53], particularly with respect to head and neck cancer and lung cancer. The advantage of PET/CT imaging in pediatric oncologic imaging has also been recently demonstrated [54–58]. We have also found PET/CT examinations in the head and neck region allow better anatomic localization and differentiation of hypermetabolic foci in the head and neck region that correlates with normal anatomic structures demonstrating brown fat or normal physiologic function (Figs. 3 and 4). PET/CT imaging can also be used to stage, localize and evaluate treatment effect in Hodgkin's disease in the neck and spine region (Figs. 5 and 6). Other examples of added value of the combined PET/CT images include better anatomic localization of hypermetabolic foci in Hodgkin's disease lymph nodes not considered significant due to CT size criteria or may be difficult to see on CT (Fig. 7). We also found that PET/CT improved the ability to detect tumor recurrence of other tumor types besides lymphoma (for example, parathyroid carcinoma), particularly with respect to lymph nodes which were not considered significant by CT size criteria. Now that combined PET/CT imaging has become more widely available, particularly in children hospitals, it will be the preferred imaging tool in the staging of lymphoma and other pediatric oncologic diseases.

PET/CT imaging of pediatric brain tumors

There has been a recent increase in the use of PET in the evaluation of brain tumors. There has also been a recent increase in radiopharmaceuticals for PET tumor imaging. Currently, FDG is the only radiotracer approved by the Food and Drug Administration (FDA). Labeled amino acids can be complementary to PET imaging. One of the most common labeled amino acids is 11C-methionine (MET). Another radiotracer, thymidine, has been shown to be useful in the evaluation of tumor proliferation [59]. FDG-PET is being used as an adjunct tool in cases where CT and MR are unable to address a specific clinical question. Most of the applications of PET to brain tumor imaging have been in adults rather than children. The most common clinical reasons for using PET imaging include: (a) confirmation of the presence or absence of tumor; (b) help in establishing the grade of malignancy; (c) determination of the degree of treatment of the tumor or tumor response; and (d) distinguishing tumor recurrence from radiation necrosis [60] (Figs. 8, 9, and 10).

FDG-PET is very sensitive in detecting high-grade gliomas. PET imaging can be confounded by the high uptake normally seen in the cortex, resulting in less accurate detection of low-grade gliomas [61]. Of note, MET-PET imaging has a higher accuracy rate compared with FDG in the detection of low-grade gliomas [62–65]. MET-PET can be useful to perform serial delayed imaging to evaluate the washout of FDG from brain tumors, because FDG usually takes longer to wash out relative to normal surrounding brain tissue [66]. Given that there might be inflammation after treatment, it is useful to delay scanning 1–2 weeks after chemotherapy and 6–8 weeks after radiation therapy [67]. MET-PET imaging might also be useful for determining treatment response in gliomas [68, 69]. There is lower uptake in surrounding brain tissue with MET compared with FDG, which results in more accurate detection by MET of low-grade gliomas [70]. 18F-fluoro-L-phenylalanine (18F-FDOPA) PET has been shown to be more accurate than 18F-FDG-PET for imaging of low-grade tumors and evaluating recurrent tumors [71].

Of note, nearly all of these studies have been performed in adults, with very little pediatric data available. More recently, PET imaging has been integrated into pediatric multi-institutional protocols of the Pediatric Brain Tumor Consortium, which will yield useful pediatric data [72].
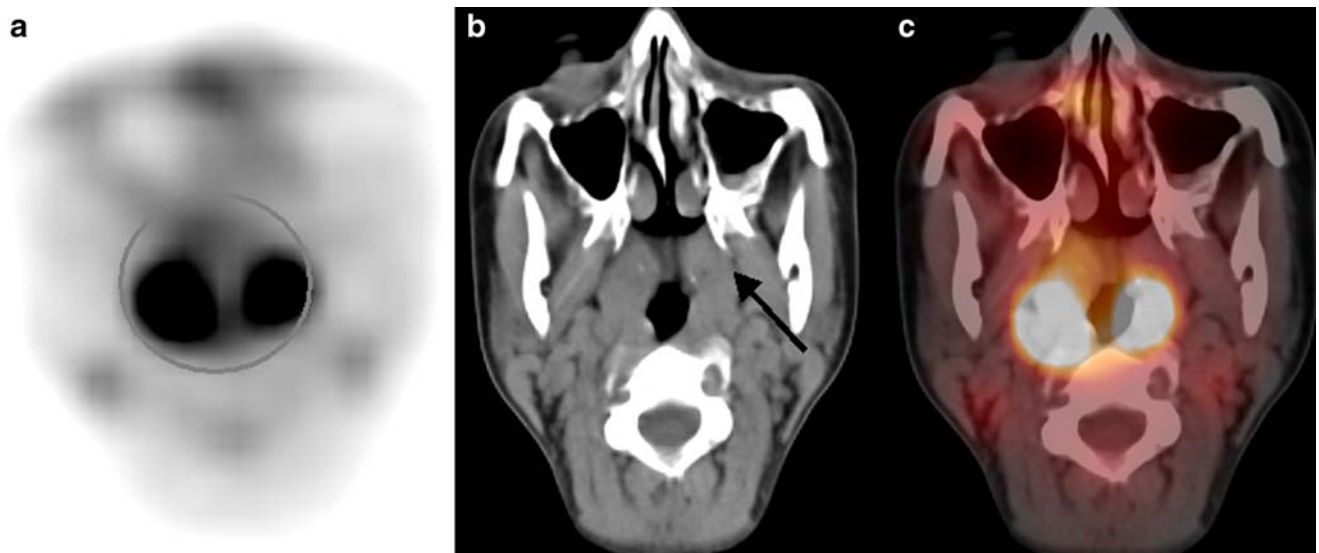
Fig. 3 Images of an 8-year-old boy with history of Hodgkin lymphoma. There is normal robust PET uptake in Waldeyer's tonsillar ring. There is mild abnormal uptake in the posterior cervical chain lymph nodes bilaterally (*black arrow*) that are not significant by CT size criteria. **a** Axial PET, **b** axial CT, and **c** fused PET/CT images

PET/MRI

With excellent soft-tissue contrast and lack of ionizing radiation, MRI has proved to be superior to CT in many indications [73–75]. A large variety of protocols including dynamic contrast-enhanced imaging, diffusion imaging, functional MRI (fMRI), MRS and the exceptionally high sensitivity of PET in the picomolar range allows PET/MRI to provide MRI information on both anatomy and function for correlation with PET-derived pathology-specific quantitative information on different aspects of tissue function [76].

However, combining two imaging modalities without compromising the optimal performance of each modality is difficult. The electronic signal pulses of PET and MRI are prone to distortion with subsequent degradation of performance.

Other challenges of integrating the two modalities are space restrictions and the difficulty in operating conventional photomultiplier tubes (PMTs) in PET in the presence of a magnetic field [77]. The hardware components of the PET detector can interfere with the performance of the MRI subsystem by degrading the homogeneity of the MRI's main magnetic field and the radio frequency (RF) field, leading to loss of image quality and causing artefacts.

At the same time, the variable MR gradients can induce currents in conductive materials of the PET detector, producing image artefacts caused by signal distortion and actual destruction of sensitive PET electronics, which, in turn, can distort the effective applied gradient field. The electronic paths between the dynodes in the PMT are deflected from its normal trajectories by the interaction with the strong external magnetic field caused by the Lorentz force.

Several alternative approaches have been proposed. One is to align PET and MRI side-by-side. This approach would require significant modifications, such as making PET detectors insensitive to the magnetic field so they would not negligibly affect the performance of the MRI scanner. Using this approach, synchronous data acquisition would not be possible and total exam time would be significantly prolonged given relatively long acquisition of both PET and MRI.

To overcome mutual interference between PET and MRI, several new approaches have been suggested:

(1) Optic fiber

To minimize electron deflection in PMT by the strong magnetic field, light fibers are designed to be coupled to the PET detector's scintillation crystals. Therefore, only coincident photon detectors remain in the magnetic field of the MR scanner and the scintillations are directed out of this high magnetic field by the light fibers. It was shown that bismuth germanate (BGO) and lutetium ortho-oxysilicate (LSO) crystals produce only small magnetic distortion, whereas gadolinium orthosilicate (GSO) and lutetium gadolinium orthosilicate cause significant distortion and artefacts in MR images [78].

Early PET/MR images showed no significant artefacts or image distortion either in PET or MRI by using 48 LSO crystals PET and 0.2–4.7 T MRI [79]. However, downsides of this method are the physical constraint of axial field-of-view and assembly issues caused by the number of optic fibers connected to each scintillation crystal and loss of light signal compared with the original amount available at the crystal's readout surface, which cause degradation of

Fig. 4 Images of a 13-year-old girl with history of Hodgkin lymphoma. There is abnormal PET uptake (*gray arrows*) in the posterior soft tissues of the neck that corresponded to fat density on the CT images. **a** Axial PET, (**b**) axial CT, and (**c**) fused PET/CT images, (**d**) coronal reformatted image of the high uptake seen at the neck base consistent with brown fat, (**e**) biopsy specimen of brown fat
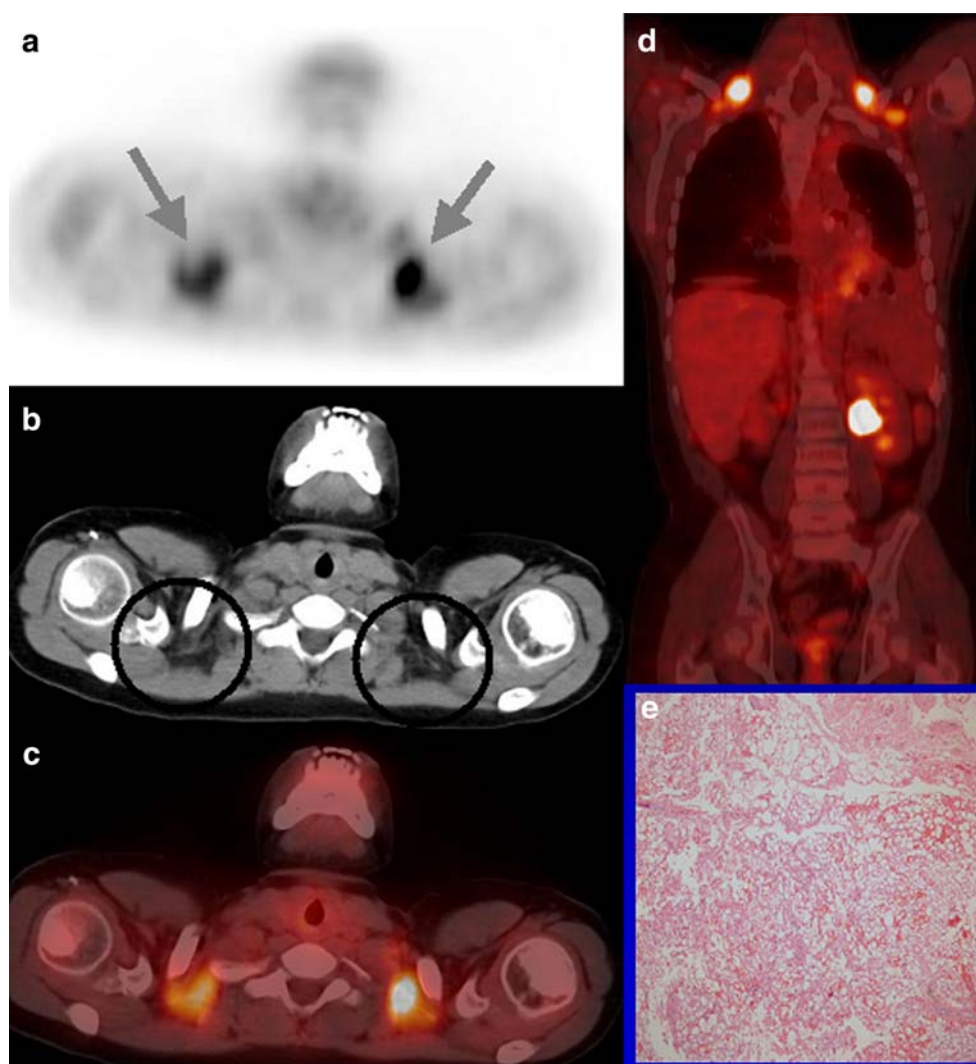
timing, energy resolution and overall PET performance [80].

(2) Semiconductor light detector

Avalanche photo dinodes (APD) have been introduced as an alternative to existing PMT for PET/MRI. Although APDs have a lower gain and are more sensitive to temperature variations than conventional PMT, the major advantage of APDs is that their insensitivity to magnetic fields allows them to be directly connected to the scintillation crystal block within the magnetic field via short light guide [81]. Therefore, light loss can be minimized and the conversion of light to electronic signals occurs inside the MR subsystem, without the use of unnecessary fragile and bulky optical fibers. In addition, a more compact design is possible by using APDs that are smaller than PMTs, leading to expansion of the axial and transaxial fields-of-view of the PET subsystem.

Because of low-gain APDs, amplification of low-amplitude analogue signal is required by using a preamplifier that is installed proximal to the APDs. Thin copper shielding is essential to prevent electrical interference of the PET system by MR and distortion of MR images by PET electronic signals. However, the copper shield itself is prone to the induction of current caused by the MR gradient system. This current can lead to MR image distortion, a reduction of the effective gradient strength and possible heat generation inside the shielding material. In the future, new semiconductor-based light detectors, such as Geiger-mode APDs (also known as silicon PMTs), will likely be developed.

(3) Split magnet

Lucas et al. [82] developed a PET system within the gap between magnets. The multi-ring PET detectors with 120-cm long optical fibers are assembled in an 80-mm gap between magnets with field strength of 1 [82]. These optic fibers connect LSO crystals of the PET detector ring inside the MR subsystem to PMTs outside the magnet. Unlike previous optic fiber design, the fibers in this design are led outside the MRI sub-system in a radial pattern rather than an axial
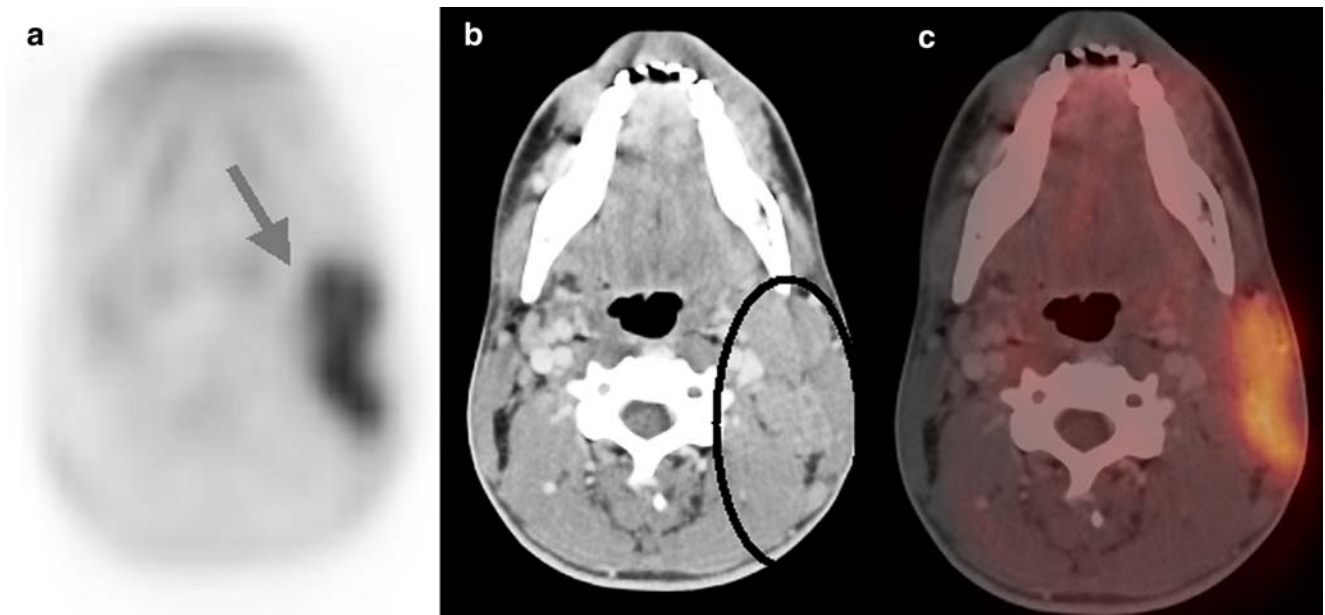
Fig. 5 Images of a 10-year-old boy with history of Hodgkin lymphoma with abnormal left jugulo-digastric and posterior cervical lymphadenopathy. The contrast-enhanced CT images do not preclude visualization of the abnormal PET uptake within the lymphadenopathy. **a** Axial PET, (**b**) axial CT, and (**c**) fused PET/CT images

direction. It was shown that successful, simultaneous PET and MR imaging could be performed using this system [82, 83]. However, there is light loss by 60% from transferring through the optic fiber, resulting in degradation of energy and time resolution. Also the limited magnetic field strength, diminished homogeneity of the main magnetic field and limited gradient performance are the shortcomings of a split magnet design.

(4)   Field cycling

Gilbert et al. [84] proposed a combination of PET and field-cycled MR where the PET subsystem can be installed in the gap of the polarizing magnet and the PET data are only acquired when both magnetic fields (polarizing field and readout fields) are off (sequential PET and MR data acquisition). One of the advantages of this method is that

Fig. 6 Lymphoma involving the thoracic spine in a child. **a** Pre-therapy sagittal T1 image shows abnormal low T1 signal within a lower thoracic vertebra consistent with lymphomatous involvement. After multiple rounds of chemotherapy, the follow-up PET/CT imaging shows hypometabolism with the same vertebra. **b** Axial PET, (**c**) axial CT, and (**d**) fused PET/CT images
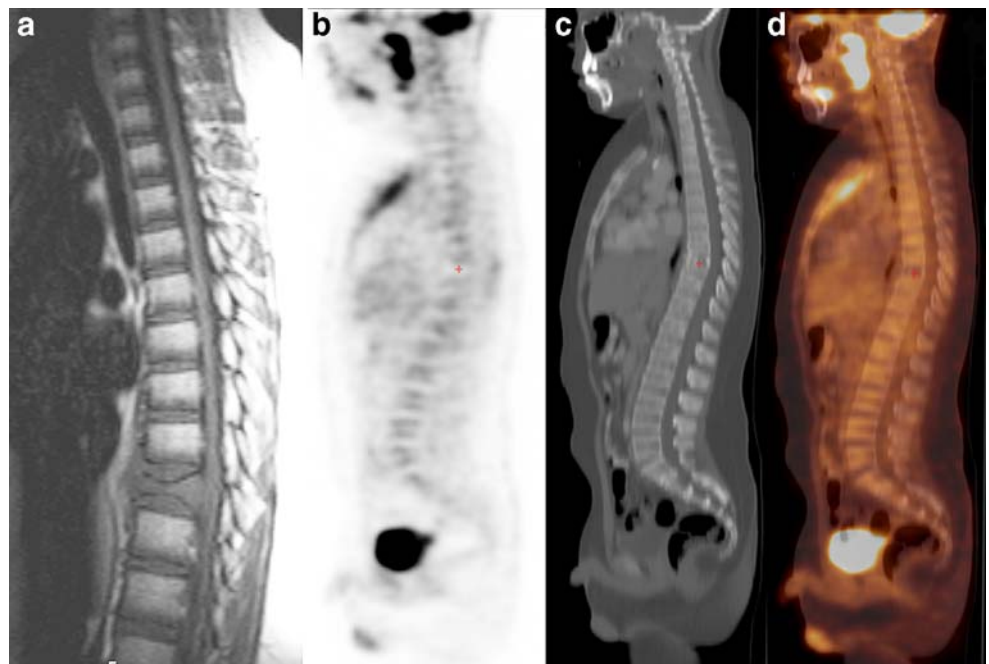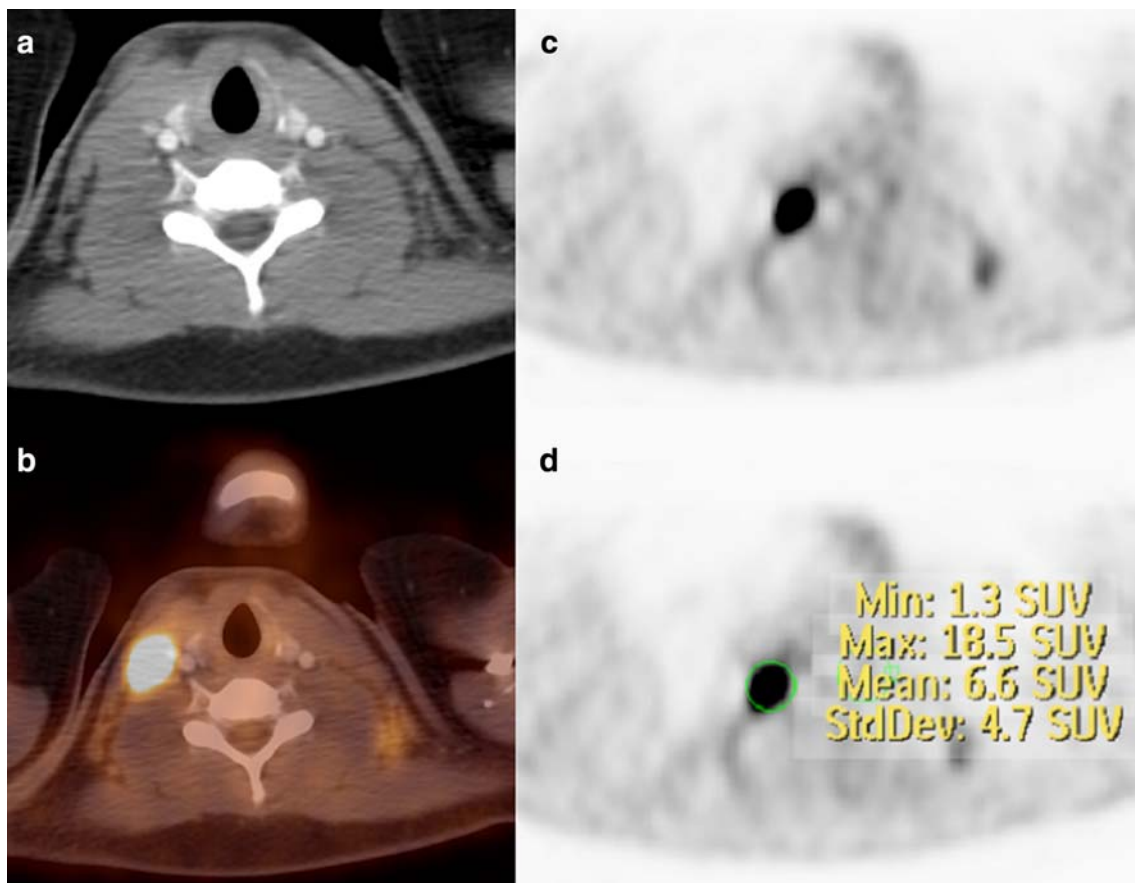
Fig. 7 Recurrent cervical lymphoma in a child. **a** CT shows no obvious lymphadenopathy. **b** The PET image shows a large focus of hypermetabolic uptake in the right posterior cervical chain region. The fused PET/CT image shows the areas of hypermetabolism co-localized with a posterior cervical chain lymph node posterior to the sternocleidomastoid muscles. **c**, **d** SUV values measured within the lymph node are suggestive of recurrent disease

no optical fibers are needed and that PMTs can be installed in the vicinity of the scintillation crystals, avoiding excessive light loss [85].

However, it is difficult to monitor temporal biological processes with non-simultaneous data acquisition. Also, it remains unclear whether the PMT performance would be compromised over time because of the relatively high magnetic fields switching at a high frequency.

Application of PET/MRI

With excellent soft-tissue differentiation, lack of ionizing radiation from the MRI component and potential simultaneous anatomical and functional data acquisition, combined PET/MRI seems promising and can offer potential application for novel molecular imaging.

Currently, most of the initial PET/MRI imaging has been based on small animal studies. The first PET/MRI studies in humans demonstrated an excellent simultaneous non-degraded performance of both PET and MRI imaging [86, 87].

A recent study showed the diagnostic advantages of fused PET and MR images over PET/CT [88]. The impact and application of PET/MRI would be greater in the neurologic and psychiatric area than any other, given various applications of MRI in these fields. With the ability of PET/MRI to obtain multiparameter functional data, kinetic studies in neurology and psychiatry can offer a variety of information on the dynamic tracer, drug, neurotransmitter and receptor distribution in various brain structures from PET with flow-dependent kinetics measured by MRI, with further extension to MRS and fMRI. Combined PET/MRI imaging might also lower the radiation exposure to children compared to PET/CT imaging.

Neuroreceptor imaging

Receptors in the brain have multiple distinct functions, such as (1) being effector sites of neurotransmission at the postsynaptic membrane, (2) having a regulatory role on presynaptic sites for transmitter uptake, and (3) providing both feedback and modulation of various functions on cell
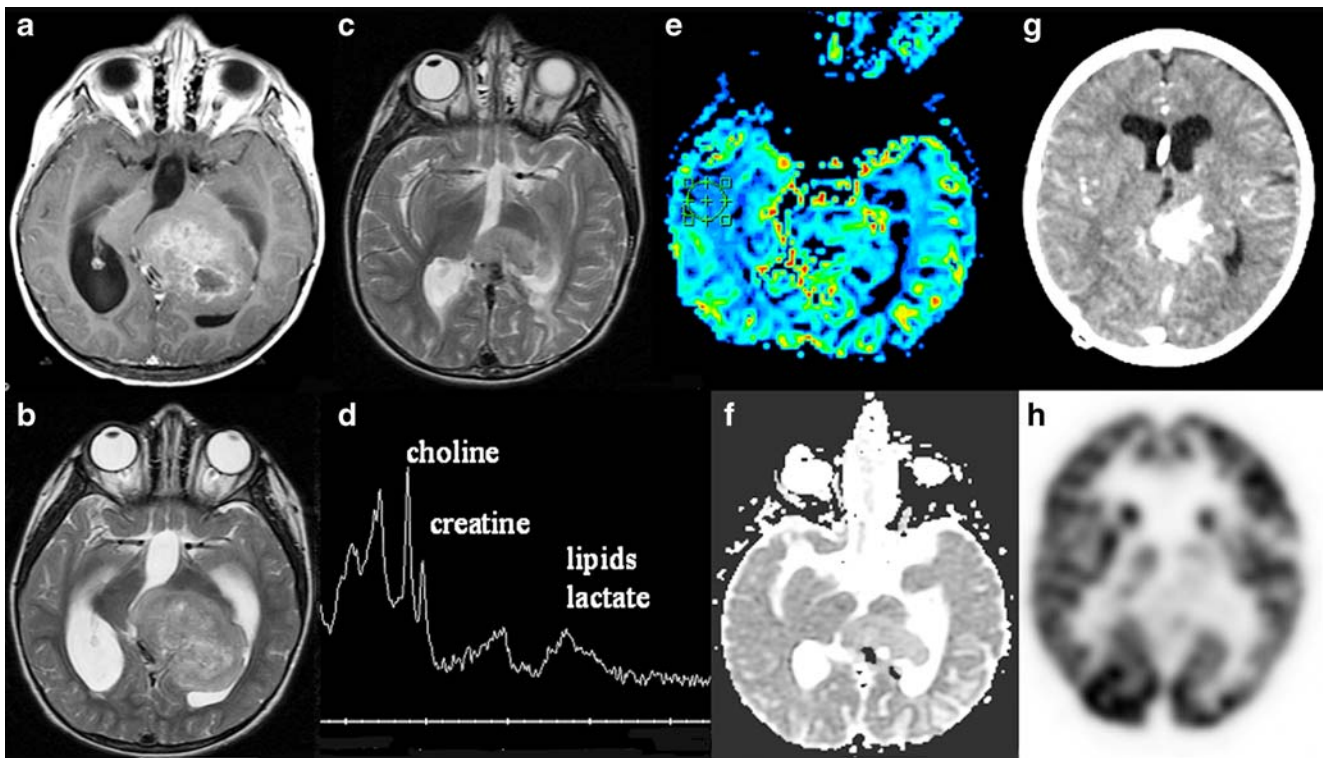
Fig. 8 Images of a child with a history of anaplastic astrocytoma involving the midbrain and thalamus. **a** Axial post-contrast T1 image shows heterogeneously enhancing mass in the region of the midbrain and thalamus. **b** Corresponding axial T2 image shows intermediate T2 heterogeneous signal within the mass. **c** After multiple rounds of chemotherapy, a smaller residual mass is seen in the same region, which had been stable over multiple scans. **d** Single-voxel MR spectroscopy of the residual tumor shows elevated myo-inositol and choline with residual NAA. **e** Dynamic contrast perfusion MR image shows relatively low cerebral blood volume within the lesion. **f** Mean diffusivity map (ADC) from diffusion tensor acquisition shows relatively higher ADC signal within the lesion compared to surrounding normal tissue, suggesting a lack of very hypercellular tumor. **g** CT from PET/CT study shows calcification within the residual tumor; **h** the corresponding PET from the PET/CT study shows relative hypometabolism within the lesion

membrane. Imaging of the distribution of receptors provides insight into the neurobiological aspects of the brain that cannot be visualized by anatomical imaging or functional imaging of blood flow and metabolism [89]. In the past, visualization of this network of various receptor systems had been limited with lack of proper radioligand and had been only demonstrated by postmortem autoradiography. However, the recent development of new radioligands makes it possible to visualize and quantify the distribution, density and activity of receptors using in vivo imaging. Up to date, PET is found to be the most selective and sensitive method (pico- to nanomolar range) for measuring receptor density and interaction in vivo.

Neuroreceptor imaging in epilepsy

Neurochemical characterization of the cortical zones in the epileptic brain with specific receptor ligands is gaining more recent attention. Currently, no studies demonstrate the clinical usefulness and superiority of receptor imaging over ictal perfusion SPECT and brain FDG-PET imaging in epilepsy. In addition, imaging of these receptors is more

limited to the research domain because of less availability compared to FDG-PET and SPECT perfusion tracers.

γ-*Aminobutyric acid (GABA)*

GABA is an inhibitory neurotransmitter in the brain that counterbalances neuronal excitation. The γ-aminobutyric acid (GABA$_A$) receptor has gained clinical significance as a marker of neuronal integrity in neurodegenerative disorder, epilepsy and stroke. It has been recently demonstrated that GABA plays an important role in the mechanism and treatment of epilepsy [90]. Among two types of GABA receptors (GABA$_A$ and GABA$_B$), GABA$_A$ receptor has been imaged using 11C- or 18F-labeled flumazenil (FMZ).

More recently, ^{11}C -labeled FMZ binding has been found to be abnormal in both gray and white matter structures in the brain of patients with different types of refractory neocortical focal epilepsy and normal MRI. Increased FMZ binding was also noted in the periventricular region, a common location for nodular heterotopia, which is associated with a poor surgical outcome in patients with unilateral hippocampal sclerosis [91]. Increases in FMZ binding in the frontal and
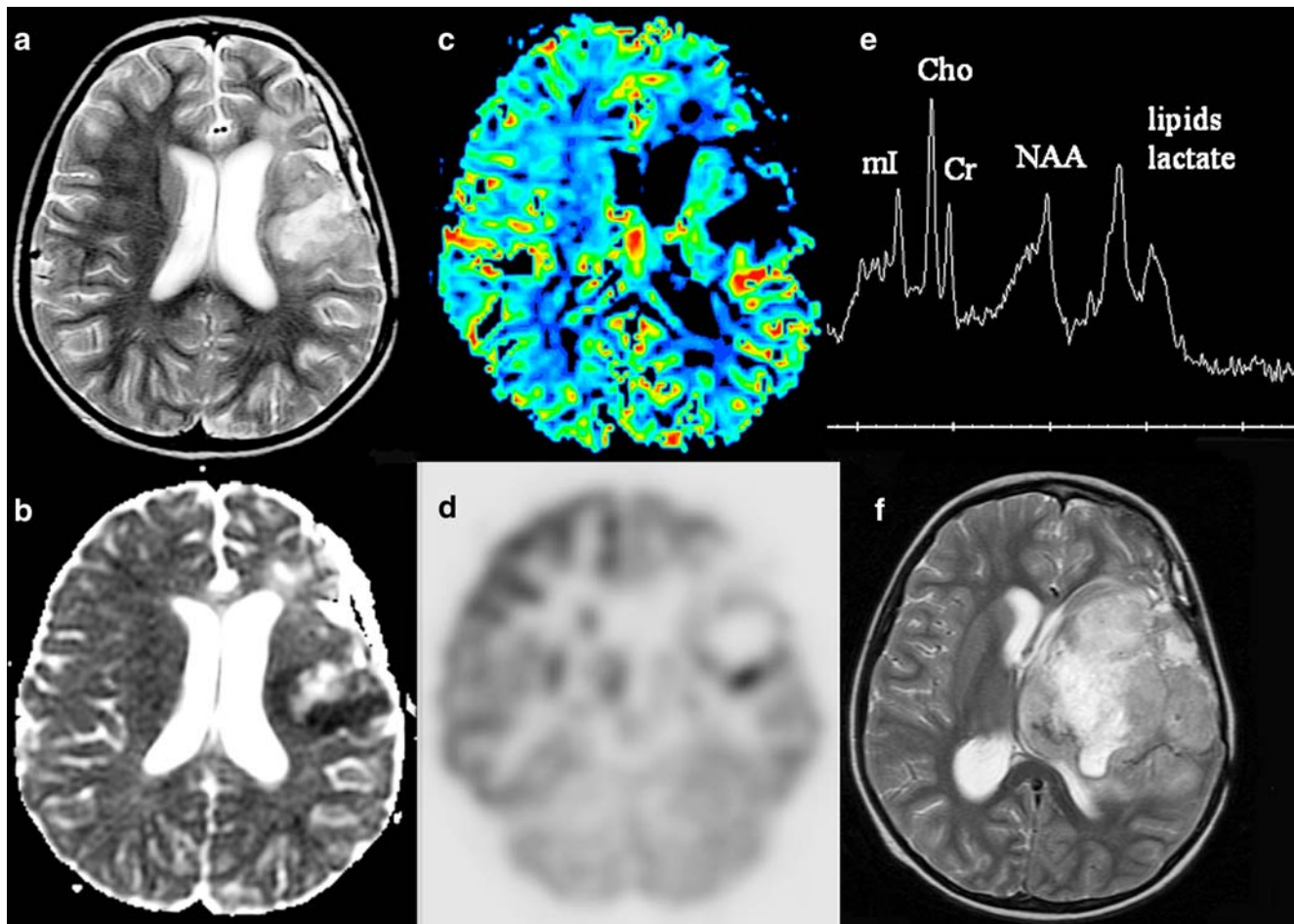
Fig. 9 Images of a child with history of anaplastic astrocytoma involving the left frontal parietal region. **a** Axial T1 image after surgical resection and multiple rounds of chemotherapy and radiation shows nonspecific edema along the margin of the resection cavity. **b** Axial mean diffusivity (ADC) image from diffusion tensor acquisition at the same time shows low ADC signal around the margin of the resection cavity, suggestive of hypercellular tumor. **c** Dynamic contrast perfusion cerebral blood volume map done at the same time shows high relative cerebral blood volume along the posterior margin of the resection cavity. **d** Corresponding PET image shows focus of hypermetabolism along the margin of the resection cavity. **e** MR spectroscopy performed at the same time along the posterior margin of the resection cavity shows elevated choline, reduced NAA and marked elevation of lipids, suggestive of transformation to glioblastoma multiforme. **f** Follow-up MR a few months later shows severe recurrence of the lesion

parietal lobes were also demonstrated in patients with parietal epilepsy [92].

Opioid receptor

There is growing evidence on the potential role of opioid in the defense mechanism as an endogenous anticonvulsant substance [93].

Frost and Mayberg et al. [94, 95] demonstrated increased binding of selective μ-opioid receptor ligand, ^{11}C-carfentanil, in the lateral temporal neocortex ipsilateral to the epileptogenic focus in patients with TLE. This is considered to be a result of an increase in affinity or the number of unoccupied receptors. A similar result was reported using δ-opioid peptide receptor ligand, ^{11}C-methylnaltrindole [96].

Increased opiate receptors in the temporal neocortex might represent a defense mechanism, a tonic anticonvulsant system that limits the spread of electrical activity from other temporal lobe structures. Also, Hammers et al. [97] reported that the increase opioid binding diminished over time after the seizure onset.

5-Hydroxtryptamine (5-HT$_{1A}$) serotonin receptor

Serotonin receptors and transporters have been studied mainly in affective disorders, Alzheimer and Parkinson diseases, autism and schizophrenia.

Converging lines of evidence implicate a potential role and association of serotonin with epilepsy in both humans and animals [98, 99]. Surgically removed human brain tissue for epilepsy showed a higher level of 5-HIAA
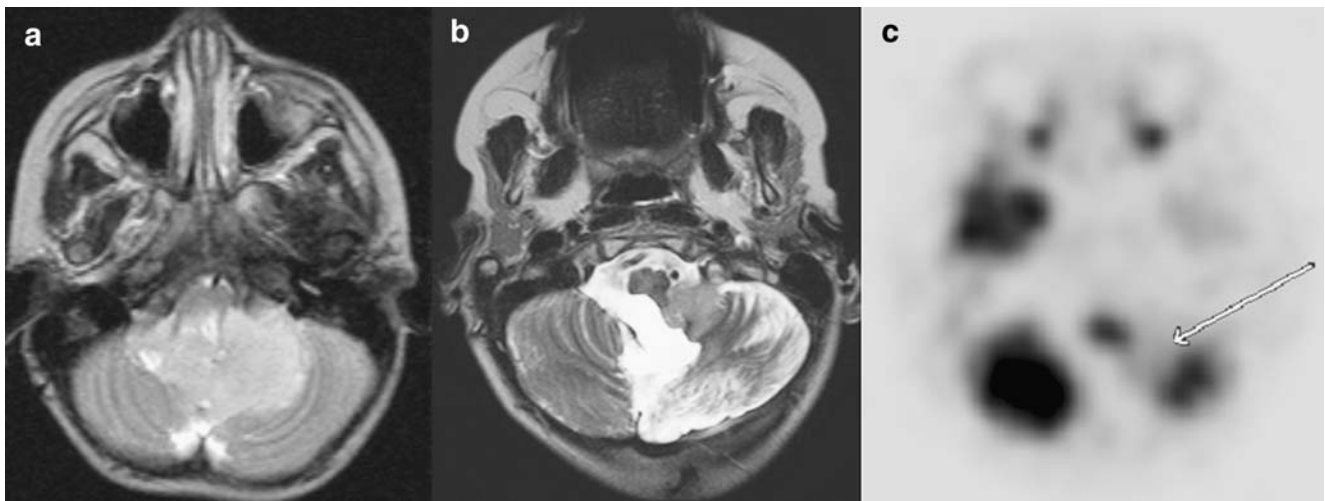
Fig. 10 A child with a posterior fossa ependymoma. **a** Axial T2 images show a posterior fossa mass centered within the fourth ventricle extending into the left foramen of Lushka, which was resected. **b** After multiple rounds of chemotherapy and radiation, a small residual focus of tissue can be seen within the left foramen of Lushka on axial T2 imaging. **c** The PET/CT image shows hypometabolism in the residual tissue, which could be metabolic inactive residual tumor or possibly scar tissue

(5-hydroxyindole acetic acid, the breakdown product of serotonin) [100, 101], and increased serotonin immunoreactivity was reported in the temporal lobe, with active spikes compared to normal control [102].

Theodore et al. [103] demonstrated reduced serotonin receptor binding in ipsilateral temporal epileptogenic foci using 18F-*trans*-4-fluoro-*N*-2-[4-(2-methoxyphenyl) piperazin-1-yl]ethyl-*N*-(2-pyridyl)cyclohexanecarboxamide (18F-FCWAY), a selective 5-HT$_{1A}$ receptor antagonist in patients with TLE, implicating decreased antagonist binding to serotonin receptor by competition of endogenous serotonin [103].

α-[11C]Methyl-L-tryptophan (AMT)

α-[11C]Methyl-L-tryptophan (AMT) is an analogue of tryptophan, a precursor for serotonin synthesis developed as a PET tracer for serotonin synthesis [104–106]. Studies have shown the increased AMT uptake of epileptogenic tubers in patients with tuberous sclerosis [107, 108].

Increased AMT uptake was more frequent in patients with cortical dysplasia (60%) than in patients with normal MRI (30%) [109]. On the other hand, Juhasz et al. [110] reported high specificity of increased AMT uptake for localizing epileptogenic lobe both in patients with normal MRI and those with cortical malformation.

It was found that the area with increased AMT uptake is adjacent to the epileptogenic focus based on spatial comparison of AMT-PET and EEG. Rosen et al. [111] demonstrated increased thalamic innervations of cortex adjacent to epileptic focus. Increased serotonin synthesis based on increased AMT uptake adjacent to epileptogenic

focus could be associated with proliferation of raphe-cortical serotonergic fiber caused by release of brain-derived neurotrophic factor from epileptogenic focus [112]. This finding led to a hypothesis of reorganization of thalamocortical afferent input where adjacent normal cortex receives relatively more innervations because of lack of target within the dysplastic epileptogenic focus.

Nicotinic acetylcholine receptor (nAChR)

Nicotinic receptor has been targeted as a marker of cognitive and membrane impairment and has been studied in depression, cognitive and memory disorders, Alzheimer and Parkinson diseases. It was found that mutation was found in a subset of genes coding for subunits of the nAChR in autosomal-dominant nocturnal frontal lobe epilepsy (ADNFLE). About 10% of ADNFLE families demonstrate mutations in the nAChR α4 or β2 subunit, which together compose the main cerebral nAChR. Picard et al. [113] found a significant increase in nAChR density in the epithalamus, ventral mesencephalon and cerebellum, suggesting these structures mediate the pathophysiology of ADNFLE and decreased nAChR density in the right dorsolateral prefrontal region, consistent with focal epilepsy involving the frontal lobe.

Conclusion

PET has become an important tool in the evaluation of pediatric neurological disease. Both PET and PET/CT can provide useful diagnostic information in the evaluation of

pediatric epilepsy, pediatric head and neck lymphoma and pediatric brain tumors. Multi-institutional trials that incorporate PET/CT protocols will likely yield more useful information that can be applied to different pediatric neurological disease processes. Future applications include combined PET-MRI imaging and neuroreceptor imaging.

References

1. Basu S, Zaidi H, Houseni M et al (2007) Novel quantitative techniques for assessing regional and global function and structure based on modern imaging modalities: implications for normal variation, aging and diseased states. Semin Nucl Med 37:223–239
2. Minn H, Leskinen-Kallio S, Lindholm P et al (1993) [18F] fluorodeoxyglucose uptake in tumors: kinetic vs. steady-state methods with reference to plasma insulin. J Comput Assist Tomogr 17:115–123
3. Kole A, Nieweg O, Pruim J et al (1997) Standardized uptake value and quantification of metabolism for breast cancer imaging with FDG and L-[1-11C]tyrosine PET. J Nucl Med 38:692–696
4. Geworski L, Knoop BO, de Wit M et al (2002) Multicenter comparison of calibration and cross calibration of PET scanners. J Nucl Med 43:635–639
5. Westerterp M, Pruim J, Oyen W et al (2007) Quantification of FDG PET studies using standardised uptake values in multi-centre trials: effects of image reconstruction, resolution and ROI definition parameters. Eur J Nucl Med Mol Imaging 34:392–404
6. Boellaard R (2009) Standards for PET image acquisition and quantitative data analysis. J Nucl Med 50:11S–20S
7. Hoekstra CJ, Hoekstra OS, Stroobants SG et al (2002) Methods to monitor response to chemotherapy in non-small cell lung cancer with 18F-FDG PET. J Nucl Med 43:1304–1309
8. Hoekstra CJ, Paglianiti I, Hoekstra OS et al (2000) Monitoring response to therapy in cancer using [F-18]-2-fluoro-2-deoxy-D-glucose and positron emission tomography: an overview of different analytical methods. Eur J Nucl Med 27:731–743
9. Eary JF, Mankoff DA (1998) Tumor metabolic rates in sarcoma using FDG PET. J Nucl Med 39:250–254
10. Lowe VJ, DeLong DM, Hoffman JM et al (1995) Optimum scanning protocol for FDG-PET evaluation of pulmonary malignancy. J Nucl Med 36:883–887
11. Gorospe L, Raman S, Echeveste J et al (2005) Whole-body PET/CT: spectrum of physiologic variants, artifacts and interpretative pitfalls in cancer patients. Nucl Med Common 26:671–687
12. Erdi YE, Nehmeh SA, Pan T et al (2004) The CT motion quantitation of lung lesions and its impact on PET-measured SUVs. J Nucl Med 45:1287–1292
13. Chugani HT, Phelps ME, Mazziotta JC (1987) Positron emission tomography study of human brain functional development. Ann Neurol 22:487–497
14. Kennedy C, Sokoloff L (1957) An adaptation of the nitrous oxide method to the study of the cerebral circulation in children; normal values for cerebral blood flow and cerebral metabolic rate in childhood. J Clin Invest 36:1130–1137
15. Chugani HT (1992) Functional brain imaging in pediatrics. Pediatr Clin North Am 39:777–799
16. Loessner A, Alavi A, Lewandrowski KU et al (1995) Regional cerebral function determined by FDG-PET in healthy volunteers: normal patterns and changes with age. J Nucl Med 36:1141–1149
17. Chawluk JB, Alavi A, Dann R et al (1987) Positron emission tomography in aging and dementia: effect of cerebral atrophy. J Nucl Med 28:431–437
18. Miura SA, Shapiro MB, Grady CL (1990) Effects of gender on glucose utilization rates in healthy humans: a positron emission tomography study. J Neurosci Res 27:500–504
19. Koepp MJ, Woermann FG (2005) Imaging structure and function in refractory focal epilepsy. Lancet Neurol 4:42–53
20. Engel J, Brown WJ, Kuhl DE et al (1982) Pathological findings underlying focal temporal lobe hypometabolism in partial epilepsy. Ann Neurol 12:518–528
21. Henry TR, Mazziotta JC, Engel J (1993) Interictal metabolic anatomy of mesial temporal lobe epilepsy. Arch Neurol 50:582–589
22. Henry TR, Babb TL, Engel J et al (1994) Hippocampal neuronal loss and regional hypometabolism in temporal lobe epilepsy. Ann Neurol 36:925–927
23. Duncan JD, Moss SD, Bandy DJ et al (1997) Use of positron emission tomography for presurgical localization of eloquent brain areas in children with seizures. Pediatr Neurosurg 26:144–156
24. Theodore WH (1992) MRI, PET, SPECT: interrelations, technical limits, and unanswered questions. Epilepsy Res Suppl 5:127–134
25. Markand ON, Spencer SS, Anderson AR (1995) SPECT in epilepsy. J Neuroimaging 5(suppl 1):S23–S33
26. Spencer S (1994) The relative contributions of MRI, SPECT, and PET imaging in epilepsy. Epilepsia 35(Suppl. 6):S72–S89
27. Semah F, Picot MC, Adam C et al (1998) Is the underlying cause of epilepsy a major prognostic factor for recurrence? Neurology 51:1256–1262
28. Lee DS, Lee SK, Chung J-K et al (1997) Predictive values of F-18-FDG PET and ictal SPECT to find epileptogenic zones in cryptogenic neocortical epilepsies (abstract). J Nucl Med 38:272
29. Chugani HT, Shields WD, Shewmon DA et al (1990) Infantile spasms: I. PET identifies focal cortical dysgenesis in cryptogenic cases for surgical treatment. Ann Neurol 27:406–413
30. Swartz BE, Brown C, Mandelkern MA et al (2002) The use of 2-deoxy-2[18F] fluoro-D-glucose (FDG-PET) positron emission tomography in the routine diagnosis of epilepsy. Mol Imaging Biol 4:245–252
31. Debets RM, Sadzot B, van Isselt JW et al (1997) Is 11C-flumazenil PET superior to 18FDG PET and 123I-iomazenil SPECT in presurgical evaluation of temporal lobe epilepsy? J Neurol Neurosurg Psychiatry 62:141–150
32. Ho SS, Berkovic SF, Berlangieri SU et al (1995) Comparison of ictal SPECT and interictal PET in the presurgical evaluation of temporal lobe epilepsy. Ann Neurol 37:738–745
33. O'Brien TJ, Hicks RJ, Ware R et al (2001) The utility of a 3-D, large-field-of-view, PENN-PET scanner in the presurgical evaluation of partial epilepsy. J Nucl Med 42:1158–1165
34. Muzik O, Chugani DC, Shen C et al (1998) Objective method for localization of cortical asymmetries using positron emission tomography to aid surgical resection of epileptic foci. Comput Aided Surg 3:74–82
35. Lin TW, de Aburto MA, Dahlbom M et al (2007) Predicting seizure-free status for temporal lobe epilepsy patients undergoing surgery: prognostic value of quantifying maximal metabolic asymmetry extending over a specified proportion of the temporal lobe. J Nucl Med 48:776–782
36. Chugani HT, Shewmon DA, Shields WD et al (1993) Surgery for intractable infantile spasms: neuroimaging perspectives. Epilepsia 34:764–771
37. Neuroimaging Subcommission of the International League Against Epilepsy (2000) Commission on diagnostic strategies: recommendations for functional neuroimaging of persons with epilepsy. Epilepsia 41:1350–1356

38. Salamon N, Kung J, Shaw SJ et al (2008) FDG-PET-MRI coregistration improves detection of cortical dysplasia in patients with epilepsy. Neurology 71:1594–1601

39. Cohen-Gadol AA, Wilhelmi BG, Collignon F et al (2006) Long-term outcome of epilepsy surgery among 399 patients with nonlesional seizure foci including mesial temporal lobe sclerosis. J Neurosurg 104:513–524

40. Palmini A, Lüders HO (2002) Classification issues in malformations caused by abnormalities of cortical development. Neurosurg Clin N Am 13:1–16 vii

41. Palmini A, Najm I, Avanzini G et al (2004) Terminology and classification of the cortical dysplasias. Neurology 62(6 Suppl 3):S2–S8

42. Krsek P, Maton B, Korman B et al (2008) Different features of histopathological subtypes of pediatric focal cortical dysplasia. Ann Neurol 63:758–769

43. Widdess-Walsh P, Kellinghaus C, Jeha L et al (2005) Electro-clinical and imaging characteristics of focal cortical dysplasia: correlation with pathological subtypes. Epilepsy Res 67:25–33

44. Lawson JA, Birchansky S, Pacheco E et al (2005) Distinct clinicopathologic subtypes of cortical dysplasia of Taylor. Neurology 64:55–61

45. Olson DM, Chugani HT, Shewmon DA et al (1990) Electrocorticographic confirmation of focal positron emission tomographic abnormalities in children with intractable epilepsy. Epilepsia 31:731–739

46. Curatolo P, Bombardieri R, Verdecchia M et al (2005) Intractable seizures in tuberous sclerosis complex: from molecular pathogenesis to the rationale for treatment. J Child Neurol 20:318–325

47. Kalantari BN, Salamon N (2008) Neuroimaging of tuberous sclerosis: spectrum of pathologic findings and frontiers in imaging. AJR 190:W304–W309

48. Koh S, Jayakar P, Dunoyer C et al (2000) Epilepsy surgery in children with tuberous sclerosis complex: presurgical evaluation and outcome. Epilepsia 41:1206–1213

49. Cusmai R, Chiron C, Curatolo P et al (1990) Topographic comparative study of magnetic resonance imaging and electroencephalography in 34 children with tuberous sclerosis. Epilepsia 31:747–755

50. Chandra PS, Salamon N, Huang J et al (2006) FDG-PET/MRI coregistration and diffusion-tensor imaging distinguish epileptogenic tubers and cortex in patients with tuberous sclerosis complex: a preliminary report. Epilepsia 47:1543–1549

51. Lardinois D, Weder W, Hany T et al (2003) Staging of non-small-cell lung cancer with integrated positron emission tomography and computed tomography. N Engl J Med 348:2500–2507

52. Hany TF, Steinhert HC, Goerres GW et al (2002) PET diagnostic accuracy: improvement with in line PET-CT system: initial results. Radiology 225:575–581

53. Antoch G, Freudenberg LS, Stattaus J et al (2002) Whole body positron emission tomography-CT: optimized CT using oral and IV contrast materials. AJR 179:1555–1560

54. McCarville MB, Christie R, Daw N et al (2005) PET/CT in the evaluation of childhood sarcomas. AJR 184:1293–1304

55. Kaste SC (2004) Issues specific to implementation of PET-CT for pediatric oncology: what we have learned along the way. Pediatr Radiol 34:205–213

56. Shulkin BL (2004) PET imaging in pediatric oncology. Pediatr Radiol 34:199–204

57. Hudson MM, Krasin MJ, Kaste SC (2004) PET imaging in pediatric Hodgkin's lymphoma. Pediatr Radiol 34:190–198

58. Kaste SC, Howard SC, McCarville EB et al (2005) 18F-FDG-avid sites mimicking active disease in pediatric Hodgkin's. Pediatr Radiol 35:141–154

59. Shields AF, Grierson JR, Dohmen BM et al (1998) Imaging proliferation in vivo with [F-18]FLT and positron emission tomography. Nat Med 4:1334–1336

60. Van Heertum RL, Greenstein EA, Tikofsky RS (2004) 2-deoxy-fluorglucose-PET imaging of the brain: current clinical applications with emphasis on dementia. Semin Nucl Med 34:300–312

61. Di Chiro G, DeLaPaz RL, Brooks RA et al (1982) Glucose utilization of cerebral gliomas measured by [18F] fluorodeoxyglucose and positron emission tomography. Neurology 32:1323–1329

62. Sasaki M, Kuwabara Y, Toshida T et al (1998) A comparative study of thallium-201 SPECT, carbon-11 methionine PET and fluorine-18 fluorodeoxyglucose PET for the differentiation of astrocytic tumors. Eur J Nucl Med 25:1261–1269

63. Ogawa T, Inugami A, Hatazawa J et al (1996) Clinical positron tomography for brain tumors: comparison of fludeoxyglucose F18 and L-methy-C-11-methionine. AJNR 17:345–353

64. Chung JK, Kim YK, Kim SK et al (2002) Usefulness of C-11-methionine PET in the evaluation of brain lesions that are hypo or isometabolic on F-18-FDG PET. Eur J Nucl Med Mol Imaging 29:176–182

65. Jager PL, Vaalburg W, Pruim J et al (2001) Radiolabelled amino acids: basic aspects and clinical application in oncology. J Nucl Med 42:432–445

66. Spence AM, Muzi M, Mankoff DA et al (2004) 18F-FDG PET of gliomas at delayed intervals: improved distinction between tumor and normal gray matter. J Nucl Med 45:1653–1659

67. Kim EE, Chung SK, Hayne TP et al (1992) Differentiation of residual or recurrent tumors from post-treatment change with F-18 FDG PET. Radiographics 12:269–279

68. Herholz K, Kracht LW, Heiss WD (2003) Monitoring the effect of chemotherapy in a mixed glioma by C-11-methionine PET. J Neuroimaging 13:269–271

69. Galldiks N, Kracht LW, Burghaus L et al (2006) Use of 11C methionine PET to monitor the effects of temozolomide chemotherapy in malignant gliomas. Eur J Nucl Med Mol Imaging 33:516–524

70. Pirotte B, Goldman S, Massager N et al (2004) Comparison of F-18-FDG and C-11-methionine for PET-guided stereotactic brain biopsy of glioma. J Nucl Med 45:1293–1298

71. Chen W, Silverman DH, Delaloye S et al (2006) ^{18}F-FDOPA PET imaging of brain tumors: comparison study with ^{18}F-FDG PET and evaluation of diagnostic accuracy. J Nucl Med 47:6904–6911

72. Williams G, Fahey FH, Treves ST et al (2008) Exploratory evaluation of two-dimensional and three-dimensional methods of FDG PET quantification in pediatric anaplastic astrocytoma: a report from the Pediatric Brain Tumor Consortium (PBTC). Eur J Nucl Med Mol Imaging 35:1651–1658

73. Barentsz JO, Jager GJ, Witjes JA et al (1996) Primary staging of urinary bladder carcinoma: the role of MRI and a comparison with CT. Eur Radiol 6:129–133

74. Kent DL, Haynor DR, Longstreth WT Jr et al (1994) The clinical efficacy of magnetic resonance imaging in neuroimaging. Ann Intern Med 120:856–871

75. Prabhakar R, Haresh KP, Ganesh T et al (2007) Comparison of computed tomography and magnetic resonance based target volume in brain tumors. J Cancer Res Ther 3:121–123

76. Pichler B, Wehrl H, Kolb A et al (2008) Positron emission tomography/magnetic resonance imaging: the next generation of multimodality imaging? Semin Nucl Med 38:199–208

77. Casey ME, Nutt R (1986) A multicrystal two-dimensional BGO detector system for positron emission tomography. IEEE Trans Nucl Sci 33:460–463

78. Yamamoto S, Kuroda K, Senda M (2003) Scintillator selection for MR-compatible gamma detectors. IEEE Trans Nucl Sci 50:1683–1685

79. Slates RB, Farahani K, Shao Y et al (1999) A study of artefacts in simultaneous PET and MR imaging using a prototype MR-compatible pet scanner. Phys Med Biol 44:2015–2027

80. Catana C, Wu Y, Judenhofer MS et al (2006) Simultaneous acquisition of multislice PET and MR images: initial results with a MR-compatible PET scanner. J Nucl Med 47:1968–1976

81. Pichler BJ, Swann BK, Rochelle J et al (2004) Lutetium oxyorthosilicate block detector readout by avalanche photodiode arrays for high resolution animal PET. Phys Med Biol 49:4305–4319

82. Lucas AJ, Hawkes RC, Ansorge RE et al (2006) Development of a combined microPET-MR system. Technol Cancer Res Treat 5:337–341

83. Lucas A, Hawkes RC, Guerra P et al (2006) Development of a combined micro-PET-MR system. IEEE Nucl Sci Symp Conf Rec 2345–2348

84. Gilbert KM, Handler WB, Scholl TJ et al (2006) Design of field-cycled magnetic resonance systems for small animal imaging. Phys Med Biol 51:2825–2841

85. Handler WB, Gilbert KM, Peng H et al (2006) Simulation of scattering and attenuation of 511 keV photons in a combined PET/field-cycled MRI system. Phys Med Biol 51:2479–2491

86. Schmand M, Burbar Z, Corbeil JL et al (2007) Brain PET: first human tomography for simultaneous (functional) PET and MR imaging. J Nucl Med Suppl 48(Suppl 2):45P Abstract 151

87. Schlemmer H-P, Pichler BJ, Wienhard K et al (2007) Simultaneous MR/PET for brain imaging: first patient scans. J Nucl Med Suppl 48(Suppl 2):45P Abstract 152

88. Muller-Horvat C, Radny P, Eigentler TK et al (2006) Prospective comparison of the impact on treatment decisions of whole-body magnetic resonance imaging and computed tomography in patients with metastatic malignant melanoma. Eur J Cancer 42:342–350

89. Heiss W, Herholz K (2006) Brain receptor imaging. J Nucl Med 47:302–312

90. Treiman DM (2001) GABAergic mechanisms in epilepsy. Epilepsia 42:8–12

91. Hammers A, Koepp MJ, Brooks DJ et al (2005) Periventricular white matter flumazenil binding and postoperative outcome in hippocampal sclerosis. Epilepsia 46:944–948

92. Hammers A, Koepp MJ, Richardson MP et al (2003) Grey and white matter flumazenil binding in neocortical epilepsy with normal MRI. A PET study of 44 patients. Brain 126:1300–1318

93. Tortella FC, Long JB (1985) Endogenous anticonvulsant substance in rat cerebrospinal fluid after a generalized seizure. Science 228:1106–1108

94. Frost JJ, Mayberg HS, Fisher RS et al (1988) Mu-opiate receptors measured by positron emission tomography are increased in temporal lobe epilepsy. Ann Neurol 23:231–237

95. Mayberg HS, Sadzot B, Meltzer CC et al (1991) Quantification of mu and non-mu opiate receptors in temporal lobe epilepsy using positron emission tomography. Ann Neurol 30:3–11

96. Madar I, Lesser RP, Krauss G et al (1997) Imaging of delta- and mu-opioid receptors in temporal lobe epilepsy by positron emission tomography. Ann Neurol 41:358–367

97. Hammers A, Asselin MC, Hinz R et al (2007) Upregulation of opioid receptor binding following spontaneous epileptic seizures. Brain 130:1009–1016

98. Toczek MT, Carson RE, Lang L et al (2003) PET imaging of 5-HT1A receptor binding in patients with temporal lobe epilepsy. Neurology 60:749–756

99. Teskey GC, Radford KS, Seif I et al (2004) MAOA knockout mice are more susceptible to seizures but show reduced epileptogenesis. Epilepsy Res 59:25–34

100. Louw D, Sutherland GB, Glavin GB et al (1989) A study of monoamine metabolism in human epilepsy. Can J Neurol Sci 16:394–397

101. Pintor M, Mefford IN, Hutter I et al (1990) The levels of biogenic amines, their metabolites and tyrosine hydroxylase in the human epileptic temporal cortex. Synapse 5:152–156

102. Trottier S, Evrard B, Vignal JP et al (1996) The serotonergic innervation of the cerebral cortex in man and its changes in focal cortical dysplasia. Epilepsy Res 25:79–106

103. Theodore WH, Hasler G, Giovacchini G et al (2007) Reduced hippocampal 5HT1A PET receptor binding and depression in temporal lobe epilepsy. Epilepsia 48:1526–1530

104. Diksic M, Nagahiro S, Chaly T et al (1991) Serotonin synthesis rate measured in living dog brain by positron emission tomography. J Neurochem 56:153–162

105. Chugani DC, Muzik O, Chakraborty P et al (1998) Human brain serotonin synthesis capacity measured in vivo with alpha-[C-11] methyl-L-tryptophan. Synapse 28:33–43

106. Muzik O, Chugani DC, Chakraborty P et al (1997) Analysis of [C-11] alpha-methyl-tryptophan kinetics for the estimation of serotonin synthesis rate in vivo. J Cereb Blood Flow Metab 17:659–669

107. Chugani DC, Chugani HT, Muzik O et al (1998) Imaging epileptogenic tubers in children with tuberous sclerosis complex using alpha-[11C]methyl- L-tryptophan positron emission tomography. Ann Neurol 44:858–866

108. Fedi M, Reutens DC, Andermann F et al (2003) alpha-[11C]-methyl-L-tryptophan PET identifies the epileptogenic tuber and correlates with interictal spike frequency. Epilepsy Res 52:203–213

109. Fedi M, Reutens D, Okazawa H et al (2001) Localizing value of alpha-methyl-L-tryptophan PET in intractable epilepsy of neocortical origin. Neurology 57:1629–1636

110. Juhasz C, Chugani DC, Muzik O et al (2003) Alpha-methyl-L-tryptophan PET detects epileptogenic cortex in children with intractable epilepsy. Neurology 60:960–968

111. Rosen GD, Burstein D, Galaburda AM (2000) Changes in efferent and afferent connectivity in rats with induced cerebrocortical microgyria. J Comp Neurol 418:423–440

112. Chugani DC (2004) Serotonin in autism and pediatric epilepsies. Ment Retard Dev Disabil Res Rev 10:112–116

113. Picard F, Bruel D, Servent D et al (2006) Alteration of the in vivo nicotinic receptor density in ADNFLE patients: a PET study. Brain 129:2047–2060